A Strengthening Mechanism and Influencing Factors of Coal Fly Ash using Microbial-Induced Carbonate Precipitation

Shuaifeng Wu
China Institute of Water Resources and Hydropower Research
Hong Cai
China Institute of Water Resources and Hydropower Research
Ran Wei
China Institute of Water Resources and Hydropower Research
Jianzhang Xiao (xjz2006@sina.cn)
China Institute of Water Resources and Hydropower Research https://orcid.org/0000-0002-7927-1203
Jun Yan
China Institute of Water Resources and Hydropower Research
Ziwen Wang
China Institute of Water Resources and Hydropower Research

Research Article

Keywords: Coal fly ash, Microbial-induced carbonate precipitation, Strengthening mechanism, Influencing factor, Experimental study

Posted Date: June 21st, 2021

DOI: https://doi.org/10.21203/rs.3.rs-501149/v1

Abstract

Coal fly ash (CFA) that is discharged from coal-fired power plants has characteristics of fine particles, a small specific gravity and a large pore ratio. The dust suppression and strengthening of CFA is usually carried out by spraying water in the ash storage yard, but this practical approach is unsatisfactory. The strength of the CFA filling material affects the construction safety and operational safety of the ash dams. To carry out effective CFA material utilization and dust-pollution control, this paper applied the microbial-induced carbonate precipitation (MICP) method to enhance the strength of CFA under two curing conditions of natural evaporation (NE) and in a moisture cylinder (MC). The microbial-reaction mechanism, strengthening characteristics and influencing factors were studied. The results show that: 1) the calcium carbonate that is produced by microorganisms in the CFA is calcite, and the calcium-carbonate content increases from 7% to 18.9% and 15.3% under the MC and NE curing conditions, respectively; 2) MICP can improve the CFA strength, and the unconfined compressive strength can be increased by 6.55 times to 97.63 kPa under the MC curing conditions; 3) the solidification strength of CFA varies significantly with the concentration of $CaCl_2.2H_2O$ and CH_4N_2O nutrients. The peak stress increases initially and then decreases with an increase in nutrient salt concentration. The optimum nutrient concentration was 0.5 mol/L and 1.0 mol/L for the MC and NE curing conditions, respectively; 4) calcium carbonate that was induced by microbial reaction can reduce the water loss in the ash specimen, and allow the ash surface to form a better water-retention effect, with good prospects for dust suppression.

Introduction

China is the largest global producer of coal, with nearly 12% of total proven reserves of 114×10^9 tons. China is also one of few countries with coal as the main energy source. Primary coal demand is projected to increase from 1308×10^6 tons in 2002 to 2402×10^6 tons in 2030 (Koukouzas et al. 2006; He et al. 2012). China's largest global coal consumption and abundant utilization of coal resources has promoted the rapid development of the economy, and coal-fired power plants consume more than 50% of the coal used in China (Wang et al. 2016). The very large scale of coal-fired plants has led to huge coal fly ash (CFA) output, which reached 375×10^6 tons in 2009, and 430×10^6 tons in 2010 (He et al. 2012). As one of the largest single pollution materials of industrial solid waste in China, the total use of CFA is only ~ 30%, which wastes lots of land for backlog and stacking (Fig. 1), and has attracted increased attention in environmental protection and public health.

CFA that is discharged from coal-fired power plants has characteristics of fine particles, a small specific gravity, a large void ratio, and an easy evaporation of water in dry environments. The practical effect of surface solidification and dust suppression by extensive water irrigation is used commonly, but is ineffective, expensive, and difficult to meet the long-term effective dust-proof needs of ash storage yards. The dust-raising phenomenon of ash storage yards under natural conditions is common (Fig. 2) and serious dust pollution occurs frequently.

Dams in ash storage yards are formed by initial and later sub-dams that become filled with CFA. With an increase in service life and the continuous expansion of low-calorie coal utilization, the stacking quantity of CFA increases significantly, and sub-dam heights can be increased continuously as required. Therefore, the strength of CFA, as the main filling material, affects the dam slope stability, and has an important impact on construction and operational safety.

Compared with the increasing construction of CFA storage yards, studies on CFA strengthening, which has an important impact on dust suppression and sub-dam slope stability, are lagging behind. For better material utilization and dust pollution control of CFA, effective strength-enhancement methods must be studied, which have an important practical significance to increase stringent environmental protection requirements and rapid developments of construction and reinforce ash dam projects.

Microorganisms have characteristics of a rapid reproduction and flexible metabolism, and because of advantages of low energy consumption, variety, abundant resources and environmental friendliness, they also have an important impact on the mechanical and engineering properties of soil (DeJong et al. 2006 & 2010; Muynck et al. 2010; Soon et al., 2013; Canakci et al. 2015). Calcium that is carbonated by microbial-induced carbonate precipitation (MICP) is used mainly in sand grains (Stocks-Fischer et al. 1999; Shirakawa et al. 2011; Bernardi et al. 2014; Martinez et al. 2014; Azadi et al. 2017) and provides a porous medium with good penetration (Whiffin et al. 2007; Tobler et al. 2012) and easy grouting.

Because of their complex chemical composition of mainly silicon, aluminium and iron oxides, followed by calcium, magnesium, potassium oxides and unburned carbon, and their special mechanical properties (Koukouzas et al. 2006; Gong et al. 2016; González et al. 2017), only a few microbial strengthening studies have been reported on CFA (Kucharski et al. 2000; Dhami et al. 2012). Previous studies have shown that MICP could decrease the compressibility and hydraulic conductivity of the CFA (Safavizadeh et al. 2016 & 2018; Montoya et al. 2019), and could reduce trace-element leaching from coal ash (Montoya et al. 2012). A systematic analysis of the strengthening enhancement mechanism is insufficient. Little is known about MICP applications in CFA dust suppression and the storage yards of coal-fired power plants, and the strength characteristics and influencing factors of the microbial strengthening of CFA require further study.

By using the MICP method, this paper focused on the strength improvement of CFA, mixed with Sporosarcina pasteurii solution and different concentrations of nutrient salts. Strengthening experiments of two curing conditions of NE and MC were carried out, combined with minerals analysis, and the reaction mechanism, strength characteristics and strength-influencing factors of treated CFA were determined. This research will be valuable for the material utilization and dust pollution control of CFA in ash storage yards.

CFA

CFA was collected from Longkou coal ash storage yard of the Beijing Shijingshan coal-fired power plant, according to Standard for geotechnical testing method (GB/T 50123 – 2019), and the basic physical

properties of the untreated (UT) CFA were tested, as shown in Table 1.

Bacteria solution

Sporosarcina pasteurii, which is a chemoheterotrophic bacteria, was from the Institute of Microbiology CAS. The cells were rod-shaped, 2–3 μm in length and 0.5–1.5 μm in diameter, gram-positive, and spore-round. Optimized #136 medium was made up by 20.0 g yeast powder, 10.0 g ammonium sulfate and 1.0 mL nickel chloride per liter of water. The pH of the medium was adjusted to 9.0, and sterilized in a high-pressure steam sterilizing pot at 120 ℃ for 20 min. After inoculation, the bacteria solution was cultured in a shaking incubator at 30 ℃ and 170 r/min for 24 h. The measured data show that the initial OD_{600} of the Sporosarcina pasteurii solution was 3.70, and the urease activity was 1.86 mS/cm/min at 26.9 ℃.

Nutrient salts

The nutrients used in the experiment were $CaCl_2{\cdot}2H_2O$ (molecular weight 147.01) and CH_4N_2O (molecular weight 60.06), produced by Chemical Reagent Co., Ltd. of China Pharmaceutical Group.

To compare the strength influencing effects of CFA by the MICP, nutrient concentrations were selected as 0.10, 0.25, 0.50, 0.75, 1.00, 1.25 and 1.50 mol/L, with two parallel specimens for each group. The diameter and height of the columnar specimens were 3.91 cm and 8.00 cm, respectively, and the masses of the nutrient salts that were added to the different groups of specimens are shown in Table 2.

To compare the strengthening enhancement effect, four control CFA specimens were prepared with water addition of the same mass as the bacterial solution under the two different curing conditions.

Specimen preparation and curing

Specimen preparation was based mainly on the ASTM D2166-00 and GB/T 50123 – 2019 standards. The mass mixing ratio of dried CFA and bacterial solution in each specimen of the different test groups was 2:1, and the initial water content was 50%.

Before specimen preparation, to ensure easy demolding, an appropriate amount of Vaseline was smeared on the inside of the specimen mold. According to the designed nutrient salt concentration, during specimen preparation, the CFA was mixed with a certain amount of solid nutrients and stirred evenly. The bacterial liquid was poured into a container that was filled with CFA and nutrient salts, and stirred evenly for 10 min. Mixed specimens were added to a mold with five layers, which were compacted layer by layer with a hammer. After the final layer had been compacted, the two ends of the specimens were leveled.

Two kinds of curing conditions were used in the MC and NE, according to the requirements of GB/T 50123 – 2019, and 7-day curing remolded specimen-related tests were carried out. The measured curing temperature in the MC was 24 ℃ and the relative humidity was 75%. The specimens under natural NE curing conditions were placed on a well-ventilated windowsill of the laboratory. Meteorological data showed that the highest temperature in Beijing from May 27 to June 2, 2018 was 35 ℃ and the lowest was 16 ℃. Unconfined compression tests were carried out after 7 days of curing.

Test Result

Appearance change

The appearances of the CFA specimens that had been cured under the 7-day MC conditions are shown in Fig. 3. The surface condition differed significantly with the nutrient concentration in the MICP test. More mildew was present on the surface of the 0.5 mol/L (Fig. 4) and 0.75 mol/L specimens without any obvious distribution of mildew at a lower or higher nutrient concentration (Fig. 5). The difference in appearance indicates that a different nutrient concentration has a significant influence on the growth of microorganisms in CFA that was cured at room temperature and humidity.

The appearance of the CFA specimen that was cured under the NE condition after 7 days is shown in Fig. 6 and the surface specimens were drier than those cured in the MC. Similar to Fig. 3, the surface conditions of the CFA specimen were also significantly different. Samples at 1.00 mol/L nutrient concentration (Fig. 7) had more surface mildew, and there was no obvious mildew on the specimen surface (Fig. 8) at lower or higher nutrient concentrations, which indicates that different nutrient concentrations have different effects on the growth of microorganisms in CFA under the NE condition.

Compared with the MICP-treated specimens, the control specimens with only water added had no mildew on the CFA surface under the two curing conditions.

Reaction mechanism

During the solidification of CFA by using Sporosarcina pasteurii,bacterial metabolism produces urease with cell dry weight up to 1%, which can decompose urea into carbonic acid (CO_3^{2-}) and ammonia (NH_4^+) (formula 1). Because of the negative charge on the cell wall, Ca^{2+} in the CFA sample is adsorbed around the cell. With increasing amount of adsorption, calcium carbonate crystal with gelation is formed around the cell as the crystal nucleus (formula 2), which gradually increases and accumulates in the process of sample curing. Subsequently, a microbial-induced calcium carbonate block with certain strength is formed in CFA.

$$CO(NH_2)_2+2H_2O \rightarrow CO_3^{2-}+2NH_4^+ \quad (1)$$

$$CO_3^{2-}+ \text{Cell-}Ca^{2+} \rightarrow \text{Cell-}CaCO_3\downarrow \quad (2)$$

In particular, it can be seen from Table 1 that the particle diameter of CFA is generally small. The particles with diameter between 0.075 – 0.005 mm or smaller than 0.005 mm accounts for 81.2% and 10.2% of the total mass, respectively. The particle size is in the same order of magnitude with the monomer size of Sporosarcina pasteurii (length 2–3 μm, diameter 0.5–1.5 μm). The particle size of microbial induced calcium carbonate is close to that of CFA particles. Hence, it is more effective for connection and filling of fly ash particles and enhance the curing strength of CFA.

Minerals and SEM analysis

Mineral crystals exhibit specific X-ray diffraction patterns. The intensity of the characteristic peaks in the patterns is correlated positively with the mineral content in the specimens, and the mineral content can be calculated from the intensity of the characteristic diffraction peaks.

To compare the mineral compositions of UT- and MICP-treated CFA specimens of MC and NE, according to SY/T 5163 – 2010 (2010), the X-ray diffraction spectra of non-clay minerals were obtained on a Rigaku TTR III instrument. A comparison of the UT, MC and NE specimens is shown in Fig. 9, and the ordinary non-clay minerals analysis results are shown in Table 3.

After MICP treatment, for rich nutrients of calcium ion and nitrogen sources, the metabolism of Sporosarcina pasteurii can precipitate calcium carbonate crystals of calcite in the CFA. Figure 9 compares the UT specimens, and shows that the calcite content increased for the MC and NE curing conditions. As shown in Table 3 the content of calcite in the UT CFA was 7.0%. After MICP treatment, the calcite content reached 18.9% and 15.3%, respectively, which is an increase of 170% and 119%, respectively.

SEM/EDS images were used to explore the presence and pattern of $CaCO_3$ precipitation. In Fig. 10 (a), it can be seen that, a great number of pores are formed in the CFA samples, and the calcium carbonate crystals induced by microorganisms are distributed among the CFA particles, with varying patterns at different positions, generally in the form of bundles (Fig. 10 (b)) and short columns (Fig. 10 (c)). Since the particle size of the microbial induced calcium carbonate is close to that of the CFA particles, the calcium carbonate crystals can connect and fill the surrounding fly ash particles more effectively, and improve the curing strength. The EDS analysis confirms that the mineral observed is calcium carbonate (Fig. 10 (d)).

Water-content change

Table 4 lists the water-content change statistics of CFA specimens in the different test groups. After 7 days of curing, under the MC curing condition, the water content of the CFA specimens with only water added decreased from 50–33.75% and 33.72%, which is a decrease of 32.50% and 32.56%, respectively. In contrast, the highest water content decrease of the MICP-treated specimens from 50–36.06%, occurred in the test group with a 0.25 mol/L nutrient concentration, which is a decrease of 27.88%, with the lowest reduction in the 0.1 mol/L group, from 50–47.97%, which is a decrease of 4.06%.

Under the NE curing condition, the water content decrease in each group of specimens was similar to that in the MC, but the decrease was larger. The water content of the specimens with only water added decreased from 50–4.90% and 4.36%, respectively, which is a decrease of 90.20% and 91.28%. The highest water content decrease of the MICP-treated specimens was from 50–24.63% in the 1.25 mol/L test group, which represents a decrease of 50.74%. The lowest reduction occurred in the 0.25 mol/L group, from 50–36.70%, which is a decrease of 26.60%. The decrease in water content indicates that the use of MICP in CFA could strengthen the interparticle connection, and reduce the internal water loss. MICP-treated CFA achieved a better water retention,could worked well in the dust suppression of CFA storage yards.

Unconfined compression strength

Unconfined compression tests were performed on all 7-day cured CFA specimens in accordance with ASTM D2166-00. Tests were performed on a CMT 4304 universal testing machine (MTS Systems Corporation). The axial loading rate was 1.0 mm/min. Loading continued until the load values decreased with an increasing strain, or until a 15% strain was reached during the test.

The different colors represent different nutrient concentrations in the stress–strain curves that were obtained from the tests. The three parallel CFA specimens in the same test groups were expressed by solid line a and dotted line b and c, and the corresponding concentrations of 0.10, 0.25, 0.50, 0.75, 1.00, 1.25 and 1.50 mol/L were marked. The control specimens with no numerical value are also shown in which no bacterial solution, but only water, was added.

Figure 11 shows the test result for curing in MC. The good cementing ability of calcium carbonate produced by MICP allowed loose CFA particles to be cemented or filled during crystallization, which can improve the compressive strength simultaneously.

The comparison shows obvious peak points in the stress–strain curves of the MICP-treated specimens. A higher peak strength yields a higher corresponding strain, and the overall tendency is similar. During the initial loading stage after the test commences, the stress increases rapidly with an increase in strain and the stress–strain curve increases approximately linearly. After reaching a maximum, the specimen reaches a limit of bearing capacity with a further increase of strain, and the stress decreases rapidly with certain brittle failure characteristics (Fig. 12). For the experiment where only water is added to the control specimens, in contrast, when the axial stress reaches its peak value, the stress decreases slowly with the increase in strain, and the brittle failure characteristics are not obvious.

The unconfined peak compressive strength of the MICP-treated specimens with different nutrient concentrations is different under the MC curing condition. Table 5 shows that the maximum peak stress of 97.63 kPa occurs in the test group with a 0.50 mol/L nutrient concentration and the average peak stress of this test group was 80.70 kPa. The minimum peak stress was 23.84 kPa in the 0.10 mol/L test group with an average stress of only 26.14 kPa. The average peak stresses for the 0.10, 0.25, 0.50, 0.75, 1.00, 1.25 and 1.50 mol/L nutrient concentration test groups were 26.14, 53.45, 80.70, 68.08, 64.74, 50.53 and 45.92 kPa, respectively. The results showed that the peak stress of CFA specimens increased initially and then decreased with the increase of nutrient concentration from 0.10 mol/L. According to the maximum compressive strength, an optimum nutrient concentration existed for the MC curing condition. At this nutrient concentration, the MICP reacted more fully and the peak strength was higher.

Compared with the MICP-treated specimens, the unconfined compressive strength of the control specimens with only water added was lowest under the same curing conditions. The maximum was only 18.20 kPa, the minimum was 14.91 kPa, and the average was 16.56 kPa, which is only 63.35%, 30.98%, 20.52%, 24.32%, 25.58%, 32.77% and 36.06% of the average peak stress of the 0.10, 0.25, 0.50, 1.00, 1.25 and 1.50 mol/L of the MICP-treated specimens, respectively.

Under the NE curing condition, the stress–strain curves from the unconfined compressive tests are shown in Fig. 13. Although the stress–strain curves have obvious peak points, the overall tendency changed partially. Compared with Fig. 11, during the initial loading stage, with the increase in strain, 1.00a and 1.25a show a rapid growth of stress and an approximately linear growth. Before reaching the peak value of 1.00b and 1.50a, the growth of stress is initially fast and then becomes slow; after failure, the stress decreases rapidly with an increase in strain. However, with the increase in strain, specimens 1.00b and 1.50a appeared and another lower peak appeared after the peak value. Unlike Fig. 11, after reaching their peak value, the control specimen stress decreased rapidly with an increase in strain, and specimen b shows a lower peak value after the maximum.

Compared with the specimens cured in MC, the peak of the axial stress appears near 2% of the relatively low strain, and all specimens showed more obvious brittle failure characteristics regardless of whether bacterial solution was added or not (Fig. 14).

Under the NE curing condition, the unconfined compressive strength with different nutrient concentrations was significantly different. Table 6 shows that a maximum peak stress of 78.46 kPa occurred in the 1.00 mol/L nutrient concentration test group, with an average stress of 69.82 kPa. The minimum peak stress was 17.07 kPa in the 0.10 mol/L test group, with an average stress of 28.50 kPa. The average peak stresses of the 0.10, 0.25, 0.50, 0.75, 1.00, 1.25 and 1.50 mol/L test groups were 28.50, 35.92, 37.27, 46.06, 69.82, 51.75 and 50.04 kPa, respectively. The peak stress increased first and then decreased with an increase in nutrient concentration from 0.10 mol/L. According to the maximum compressive strength, an optimum nutrient concentration of 1.00 mol/L existed in the MICP-treated CFA under the NE curing condition. The MICP reacted more fully and the peak strength was higher for this nutrient concentration.

Compared with the MICP-treated specimens under the same curing condition, the strength of the control specimens with only water added was lowest, with a maximum of only 20.92 kPa, a minimum of 16.49 kPa, and an average is 18.70 kPa, which is only 65.61%, 52.06%, 50.17%, 40.60% 26.78%, 36.14%and 37.37% of the average peak stress of 0.10, 0.25, 0.50, 0.75, 1.00, 1.25 and 1.50 mol/L of the MICP-treated specimens.

Conclusions

1) During MICP, the metabolism of Sporosarcina pasteurii can result in the precipitation of calcium carbonate crystals in the CFA specimens, with the main precipitate being calcite. Compared with the UT specimens, the calcium-carbonate content increased from 7–18.9% and 15.3% under the MC and NE curing conditions, respectively, which represents an increase of 170% and 119%, respectively.

2) Compared with the CFA specimens with only water added, the MICP can improve the unconfined compression strength significantly regardless of the MC and NE curing conditions, and can be increased up to by 6.55 times to 97.63 kPa under the curing condition of MC.

3) The solidification strength of the CFA varies significantly with variations in $CaCl_2.2H_2O$ and CH_4N_2O nutrient concentrations. The peak stress increases initially and then decreases with an increase in nutrient salt concentration. The optimum nutrient concentrations were 0.50 mol/L and 1.00 mol/L under the MC and NE curing conditions, respectively.

4) Calcium carbonate induced by microbial reaction can reduce the loss of water in the ash specimen, and allow the ash surface to achieve a better water-retention effect, with good application prospects in dust suppression and seepage control of ash dams.

Declarations

Ethical Approval

NOT Applicable

Consent to Participate

NOT Applicable

Consent to Publish

NOT Applicable

Authors Contributions

Jianzhang Xiao contributed to the conception of the study;

Shuaifeng Wu, Hong Cai and Ziwen Wang performed the experiment;

Ran Wei contributed significantly to analysis and manuscript preparation;

Jianzhang Xiao and Jun Yan performed the data analyses and wrote the manuscript;

Funding

This research was supported by Independent Research Topics from the State Key Laboratory of Simulation and Regulation of the Water Cycle in River Basins (Grant number SKL2020TS05).

Competing Interests

No conflict of interest exits in the submission of this manuscript, and manuscript is approved by all authors for publication.

Availability of data and materials

The data sets supporting the results of this article are included within the article and its additional files.

Acknowledgments

This research was supported by Independent Research Topics from the State Key Laboratory of Simulation and Regulation of the Water Cycle in River Basins (Grant number SKL2020TS05). We thank Laura Kuhar, PhD, from Liwen Bianji, Edanz Group China (www.liwenbianji.cn/ac), for editing the English text of a draft of this manuscript.

References

1. ASTM. 2004. *Test specification for unconfined compressive strength of cohesive soil*. ASTM D2166-00. West Conshohocken, PA: ASTM.
2. Azadi, M., Ghayoomi, M., Shamskia, N., and Kalantari, H., 2017. “Physical and mechanical properties of reconstructed bio-cemented sand.” *Soils. Found.* 57(5):698-706.
3. Bernardi, D., DeJong, J. T., Montoya, B. M., and Martinez, B. C., 2014, “Bio-bricks: Biologically cemented sandstone bricks.” *Constr. Build. Mater.* 55:462-469.
4. Canakci, H., Sidik, W., and Kilic, I. H., 2015, “Effect of bacterial calcium carbonate precipitation on compressibility and shear strength of organic soil.” *Soils. Found.* 55(5):1211-1221.
5. DeJong, J. T., Mortensen, B. M., Martinez, B. C., and Nelson, D. C., 2010, “Bio-mediated soil improvement.” *Ecol. Eng.* 36:197-210.
6. DeJong, J. T., Fritzges, M. B., and Nüsslein, K., 2006, “Microbially induced cementation to control sand response to undrained shear.” *J. Geotech. Geoenviron. Eng.* 132(11):1381-1392.
7. Dhami, N. K., Reddy, M. S., and Mukherjee, A., 2012, “Improvement in strength properties of ash bricks by bacterial calcite.” *Ecol. Eng.* 39:31-35.
8. González, I., Vázquez, M. A., Romero-Baena, A. J., and Barba-Brioso, C., 2017, “Stabilization of fly ash using cementing bacteria. Assessment of cementation and trace element mobilization.” *J. Hazard. Mater.* 321:316-325.
9. Gong, B. G., Tian, C., Xiong, Z., Zhao, Y. C., and Zhang, J. Y., 2016 “Mineral changes and trace element releases during extraction of alumina from high aluminum fly ash in Inner Mongolia, China.” *Int. J. Coal. Geol.* 166:96-107.
10. He, Y., Luo, Q. M., and Hu, H. L., 2012, “Situation analysis and countermeasures of China’s fly ash pollution prevention and control.” *Procedia. Environ. Sci.* 16:690-696.
11. Koukouzas, N. K., Zeng, R. S., Perdikatsis, V., Xu, W. D., and Kakaras, E. K., 2006, “Mineralogy and geochemistry of Greek and Chinese coal fly ash.” *Fuel.* 85:2301-2309.
12. Kucharski, E. S., Chow, F. C., Price, G. P., Vaughan, P. R., and McGinnity, B. T., 2000, “Investigations into the stabilisation of ash using the calcite in situ precipitation system.” *Classical Rev.* 24:523-549.
13. Martinez, B. C., DeJong, J. T., and Ginn, T. R., 2014, “Bio-geochemical reactive transport modeling of microbial induced calcite precipitation to predict the treatment of sand in one-dimensional flow.” *Comput. Geotech.* 58(31):1-13.

14. Montoya, B. M., Safavizadeh, S., and Gabr, M. A., 2019, “Enhancement of coal ash compressibility parameters using microbial-induced carbonate precipitation.” *J. Geotech. Geoenviron. Eng.* 145(5): 04019018.
15. Montoya, B. M., Safavizadeh, S., and Meredith, A., 2016, “The use of microbial induced calcite precipitation to reduce trace element leaching from fly ash.” *Geo-Chicago 2016 GSP.* 271:989-997.
16. Muynck, W. D., Belie, N. D., and Verstraete, W., 2010, “Microbial carbonate precipitation in construction materials: A review.” *Ecol. Eng.* 36:118-136.
17. Safavizadeh, S., Montoya, B. M., and Gabr, M. A., 2018, “Effect of microbial induced calcium carbonate precipitation on compressibility and hydraulic conductivity of fly ash.” *IFCEE 2018 GSP.* 296:69-79.
18. Safavizadeh, S., Montoya, B. M., and Gabr, M. A., 2018, “Treating coal ash with microbial-induced calcium carbonate precipitation.” *J. Geotech. Geoenviron. Eng.* 144(11): 02818003-1.
19. Shirakawa, M. A., Kaminishikawahara, K. K., John, V. M., Kahn, H., and Futai, M. M., 2011, “Sand bioconsolidation through the precipitation of calcium carbonate by two ureolytic bacteria.” *Mater. Lett.* 65(11):1730-1733.
20. GB/T 50123-2019. 2019. *Standard for geotechnical testing method.* China Planning Press, Beijing. (in Chinese)
21. SY/T 5163-2010. 2010. *Analysis method for clay minerals and ordinary non-clay minerals in sedimentary rocks by the x-ray diffraction.* Petroleum Industry Press, Beijing. (in Chinese)
22. Soon, N. W., Lee, L. M., Khun, T. C., and Ling, H. S., 2013, “Improvements in engineering properties of soils through microbial-induced calcite precipitation.” *KSCE. J. Civ. Eng.* 17(4):718-728.
23. Stocks-Fischer, S., Galinat, J. K., and Bang, S. S., 1999, “Microbiological precipitation of $CaCO_3$.” *Soil. Biol. Biochem.* 31(11):1563-1571.
24. Tobler, D. J., Maclachlan, E., and Phoenixa, V. R., 2012, “Microbially mediated plugging of porous media and the impact of differing injection strategies.” *Ecol. Eng.* 42:270-278.
25. Whiffin, V. S., Van, Paassen, L. A. and Harkes, M. P. 2007, “Microbial carbonate precipitation as a soil improvement technique.” *Geomicrobiol. J.* 24: 417-423.

Tables

Table 1 Basic physical properties of CFA

Material	grain composition (%)			*W*		
	≤0.075mm	0.075≥0.005mm	≥0.005mm	(%)	(g/cm^3)	
UT	8.6	81.2	10.2	2	0.85	2.02

Table 2 Concentration and mass of nutrient salts in different test specimens

Nutrient concentration (mol/L)	$CaCl_2 \cdot 2H_2O$ (g)	CH_4N_2O (g)	Mixing ratio (m_{cfa}/m_{bs})	Curing time (d)
0.00	0	0	2	7
0.10	0.65	0.27	2	7
0.25	1.63	0.67	2	7
0.50	3.26	1.33	2	7
0.75	4.89	2.01	2	7
1.00	6.52	2.66	2	7
1.25	8.15	3.33	2	7
1.50	9.78	3.99	2	7

Table 3 Ordinary non-clay minerals analysis of CFA specimens

Material	Mineral content (%)				
	Quartz	Potash feldspar	Calcite	Mullite	Clay mineral
UT	8.8	5.6	7.0	75.3	3.3
MC	7.0	0.5	18.9	71.2	2.4
NE	6.0	0.6	15.3	75.2	2.9

Table 4 Water content change of CFA specimens after 7-day curing

Nutrient concentration (mol/L)	Initial water content (%)	Moisture cylinder (%)			Natural evaporation (%)		
0.00	50	33.75	33.72	-	4.90	4.36	-
0.10	50	47.97	47.95	33.14	29.02	33.03	33.14
0.25	50	45.64	46.87	35.06	36.70	35.66	35.06
0.50	50	41.90	42.16	41.43	24.65	24.87	34.91
0.75	50	43.71	43.12	42.45	26.38	24.68	35.22
1.00	50	42.83	42.40	42.22	25.70	26.44	30.54
1.25	50	42.21	40.62	40.00	25.95	24.63	31.35
1.50	50	42.15	42.36	40.98	28.06	27.71	31.10

Table 5 Unconfined compressive strength of CFA specimens cured in MC

Nutrient concentration (mol/L)	Mixing ratio (m_{cfa}/m_{bs})	Curing time (d)	Peak stress (kPa)	Average peak stress (kPa)
0.00	2	7	18.20	16.56
0.00	2	7	14.91	
0.10	2	7	26.48	26.14
0.10	2	7	28.09	
0.10	2	7	23.84	
0.25	2	7	65.80	53.45
0.25	2	7	58.37	
0.25	2	7	36.18	
0.50	2	7	97.63	80.70
0.50	2	7	76.04	
0.50	2	7	68.42	
0.75	2	7	85.27	68.08
0.75	2	7	78.07	
0.75	2	7	40.90	
1.00	2	7	62.29	64.74
1.00	2	7	74.85	
1.00	2	7	57.08	
1.25	2	7	53.37	50.53
1.25	2	7	46.10	
1.25	2	7	52.13	
1.50	2	7	34.45	45.92
1.50	2	7	49.31	
1.50	2	7	53.99	

Table 6 Unconfined compressive strength of CFA specimens cured in NE

Nutrient concentration (mol/L)	Mixing ratio (m_{cfa}/m_{bs})	Curing time (d)	Peak stress (kPa)	Average peak stress (kPa)
0.00	2	7	20.92	18.70
0.00	2	7	16.49	
0.10	2	7	39.01	28.50
0.10	2	7	29.41	
0.10	2	7	17.07	
0.25	2	7	43.42	35.92
0.25	2	7	34.02	
0.25	2	7	30.31	
0.50	2	7	25.60	37.27
0.50	2	7	45.75	
0.50	2	7	40.46	
0.75	2	7	53.87	46.06
0.75	2	7	42.87	
0.75	2	7	41.43	
1.00	2	7	78.46	69.82
1.00	2	7	73.90	
1.00	2	7	57.12	
1.25	2	7	54.13	51.75
1.25	2	7	40.67	
1.25	2	7	60.46	
1.50	2	7	45.72	50.04
1.50	2	7	44.09	
1.50	2	7	60.30	

Figures

Figure 1

CFA backlog stacking in ash storage yard of coal-fired power plant

Figure 2

Dust pollution caused by poor solidification of CFA in storage yard

Figure 3

Specimens cured in MC

Figure 4

Mildew on the surface of 0.50 mol/L specimen cured in MC

Figure 5

Mildew on the surface of 1.25 mol/L specimen cured in MC

Figure 6

Specimens cured in NE

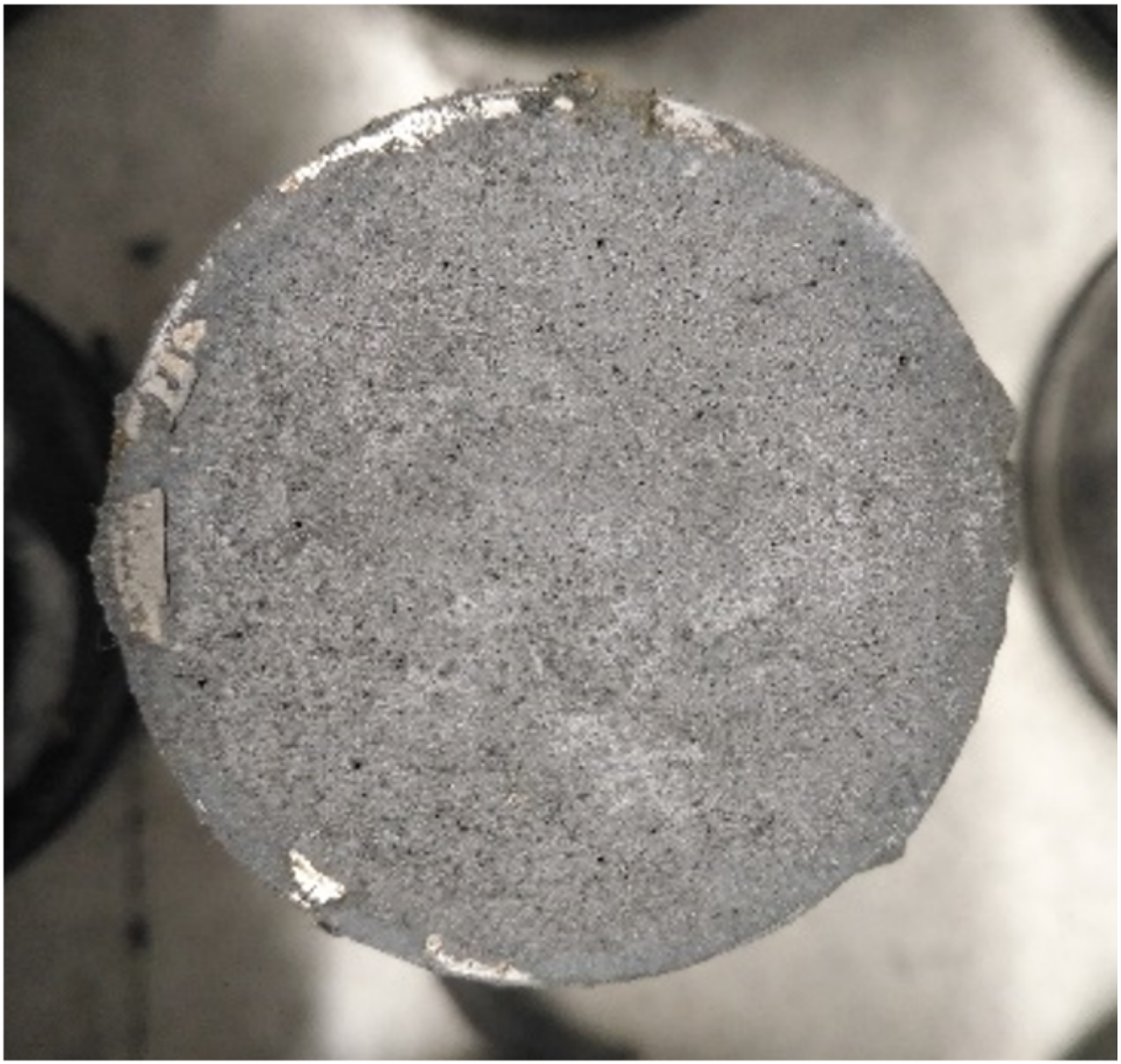

Figure 7

Mildew on the surface of 1.00 mol/L specimen cured in NE

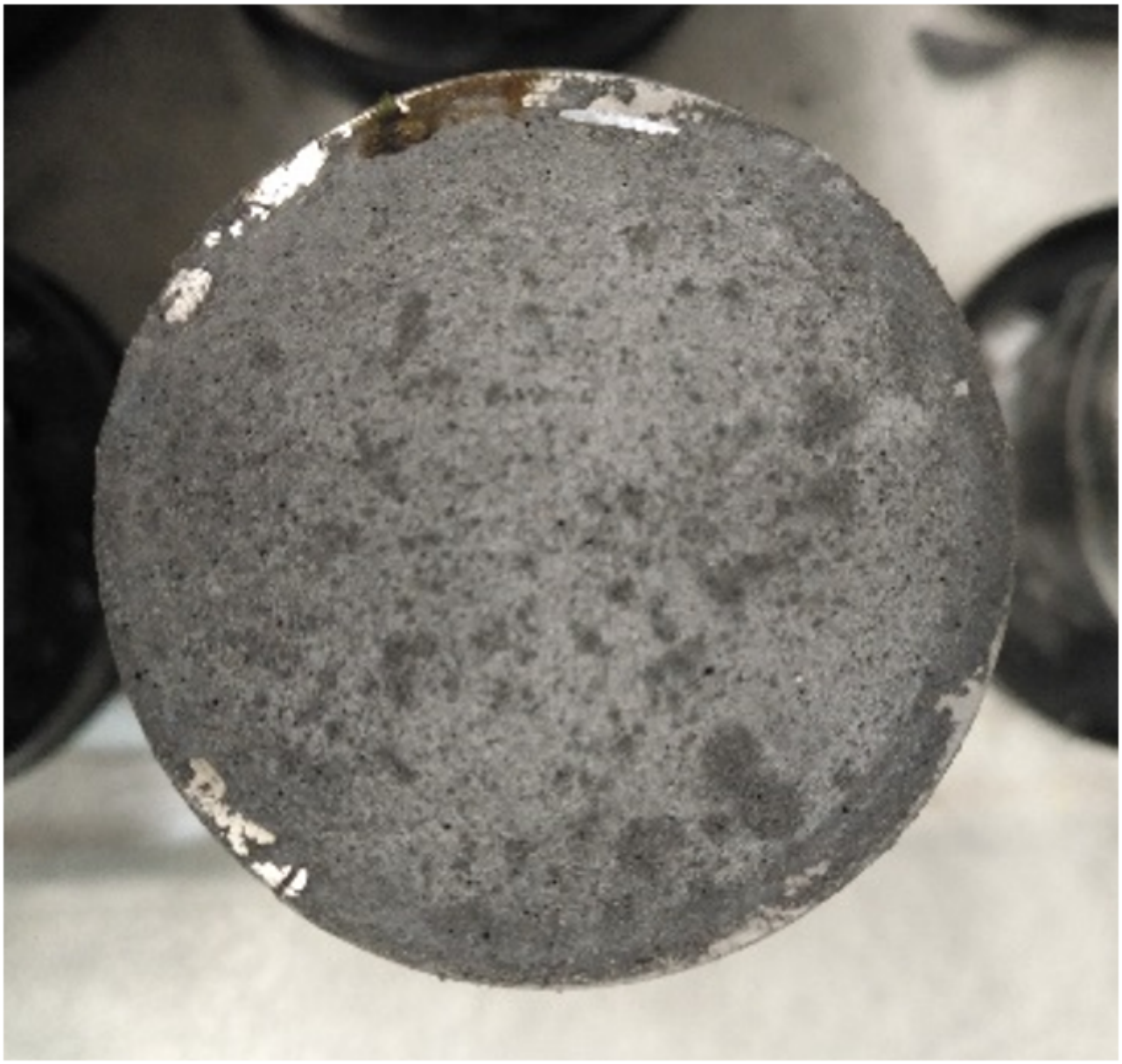

Figure 8

Mildew on the surface of 1.25 mol/L specimen cured in NE

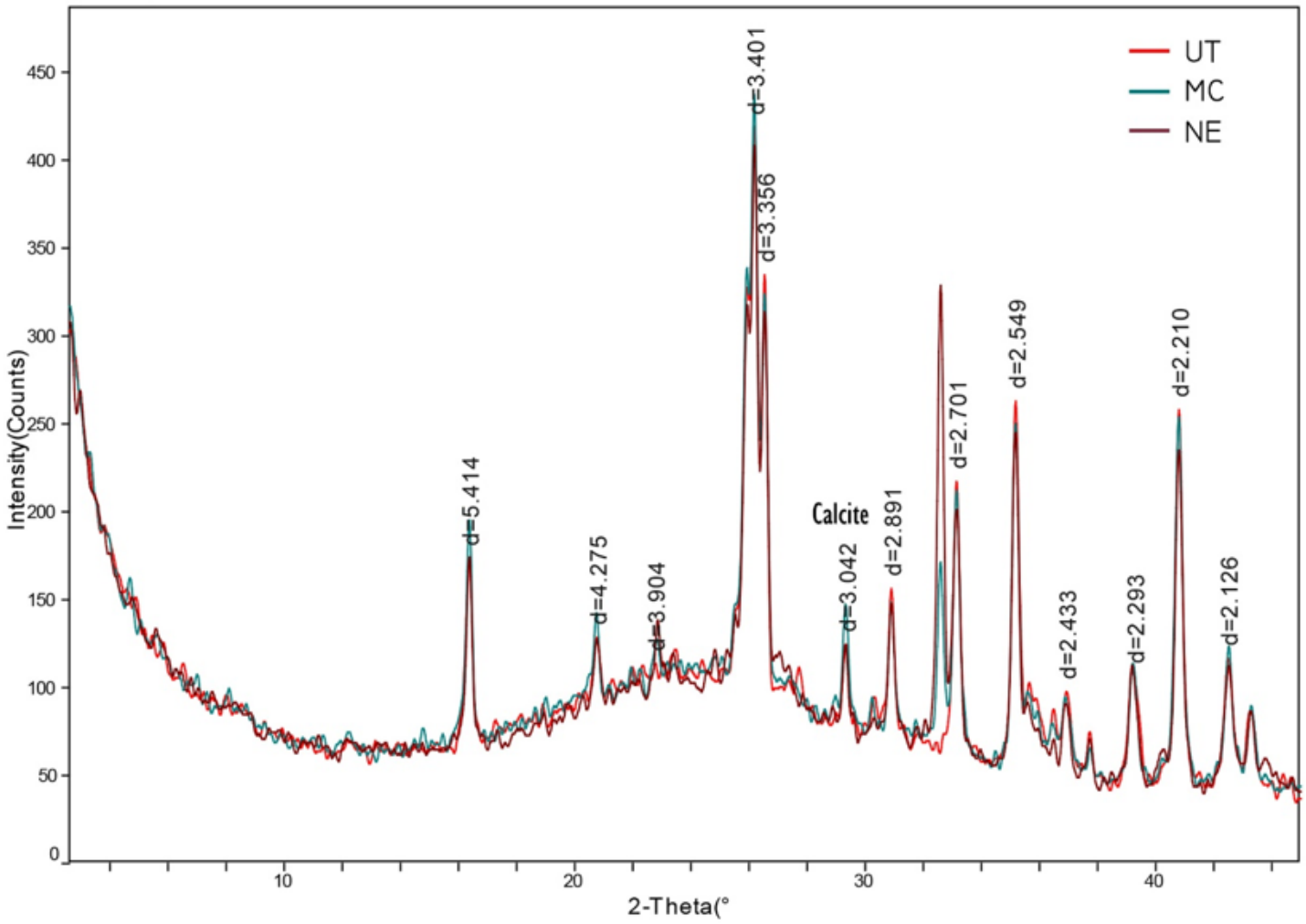

Figure 9

Comparison of X-ray diffraction spectrum of non-clay minerals of UT, MC and NE specimens

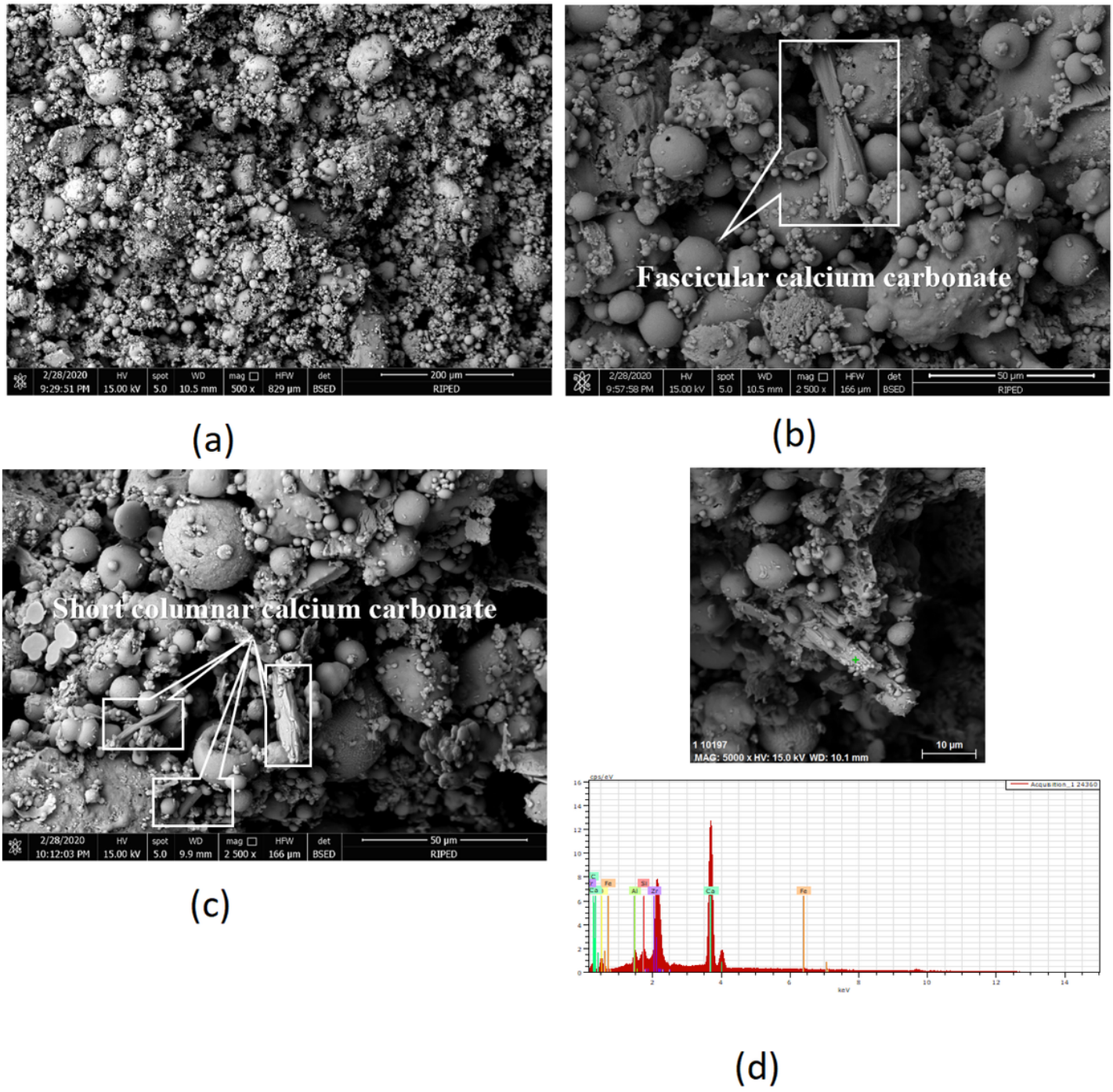

Figure 10

SEM/EDS images of treated CFA material

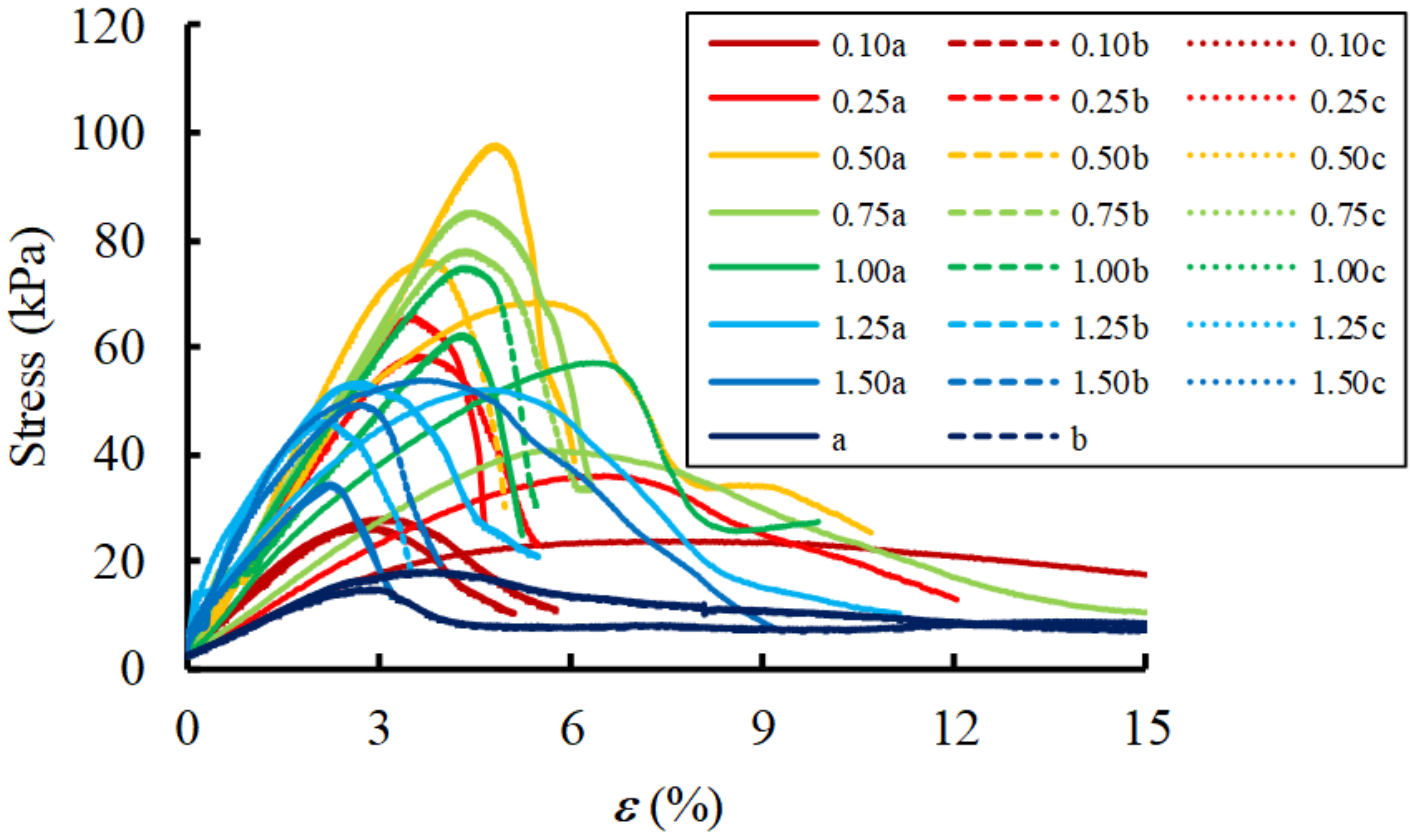

Figure 11

Stress–strain relationship curve of CFA specimens cured in MC

Figure 12

Failure of 0.50 mol/L CFA specimen cured in MC

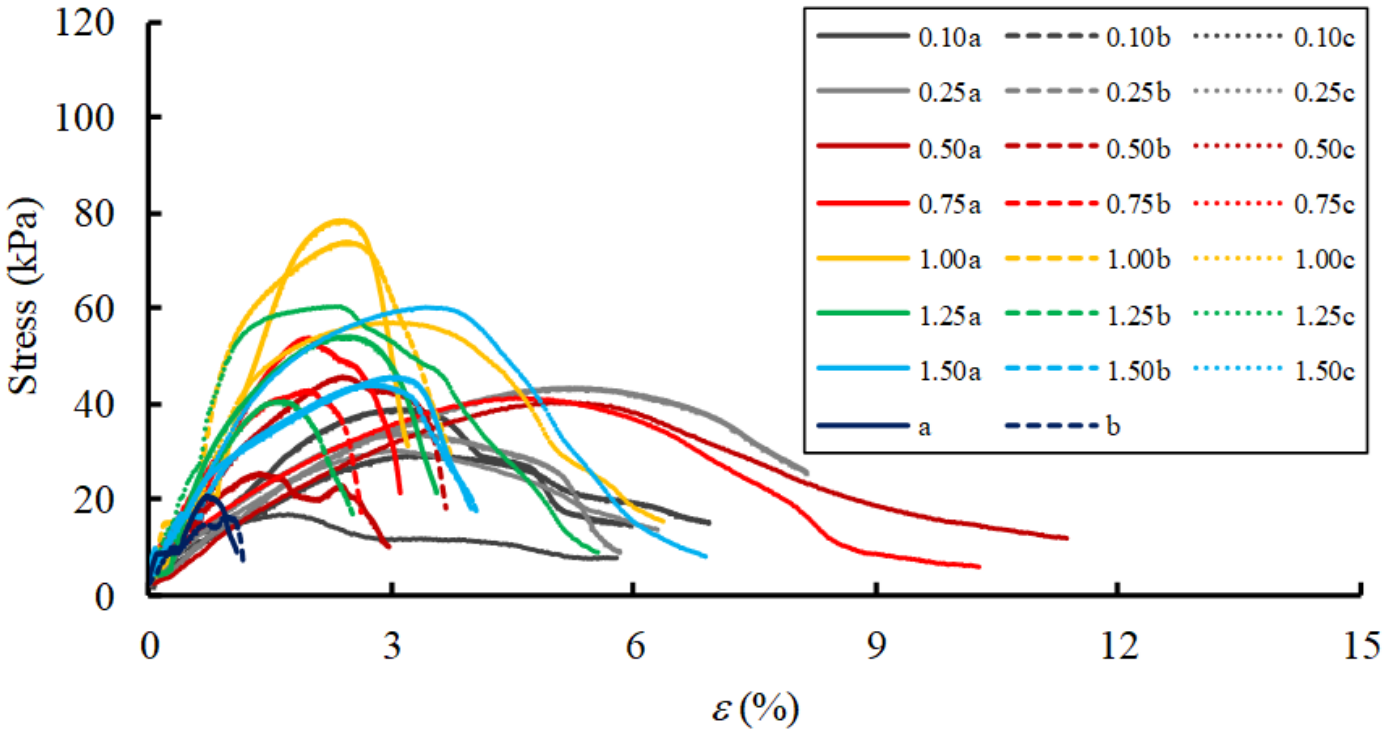

Figure 13

Stress–strain relationship curve of CFA cured in NE

Figure 14

Failure of 1.00 mol/L CFA specimen cured in NE